NATURAL CONVECTION OF A COMPRESSIBLE FLUID IN SPHERICAL LAYERS

G. B. Petrazhitskii and N. M. Stankevich

UDC 536.25

The study of convective flows of a viscous compressible fluid in spherical layers is of considerable interest for various technical applications. From the large amount of experimental material accumulated [1-4] it is possible to obtain average heat-transfer characteristics, to establish the type of flow, and to classify the flow regimes as a function of the Grashof number and the ratio of the diameters of the spheres. Scanlan et al. [3] give the temperature profiles for a wide range of Prandtl numbers. All the experimental papers are devoted to a study of convection when the inner spherical surface is the hotter. The problem was analyzed theoretically in [5, 6]. Mack and Hardee [5] studied the steady axisymmetric natural convection of an incompressible liquid between isothermal concentric spheres at low Rayleigh numbers ($Ra < 10^4$). The fundamental equations were solved by expanding the temperature T and the stream function ψ in series in powers of the Rayleigh number and estimating the first three terms in each of these series. The configuration of flow lines, the distribution of velocity and temperature, and data on heat fluxes at the spherical surfaces are given for one particular case. Similarity theory is used in [6] to obtain the heat-transfer law for natural convection in cylindrical and spherical layers, taking account of the curvature of the region. In addition to experimental and analytical methods of investigation, numerical experiment is becoming more and more important, enabling one to study rather complete physical models, to analyze in detail the effect of various parameters on the phenomena under study, and to develop the fundamental laws of the process. Numerical experiment yields the information necessary for a more thorough analysis of convective heat transfer and the establishment of the law of interaction of hydrodynamic and thermal effects, namely: the structure of the flow field, and the distribution of density, temperature, and the local heat fluxes at the boundaries of the region. It is practically impossible to obtain this information in a full-scale experiment.

The purpose of the present paper is to determine the laws of convective motion and heat transfer of a viscous compressible gas between a cooled inner spherical surface and a heated outer concentric spherical surface. It is assumed that the gas obeys the ideal gas law $p = R^*\rho T$, and that the temperature dependence of the thermal conductivity λ and the dynamic viscosity μ is given by the Sutherland formula

$$\lambda = 0.254 \cdot 10^{-2} \frac{T^{3/2}}{T + 201/\Delta T} \cdot \frac{\sqrt{\Delta T}}{\lambda_m};$$

$$\mu = 1.465 \cdot 10^{-6} \frac{T^{3/2}}{T + 110{,}4/\Delta T} \cdot \frac{\sqrt{\Delta T}}{\mu_m}.$$

The specific heat c_p depends linearly on the temperature. The only body force is gravity.

The presence of a temperature gradient in the gravitational field makes hydrostatic equilibrium impossible. The convection currents which arise in the gap exert a large effect on the heat-transfer process. The temperature distribution changes, and the rate of heating the medium in the gap is increased. The flows generated are symmetric with respect to the vertical z axis of the cylindrical coordinate system x, θ, z with its origin at the center of the concentric spherical surfaces.

The investigation of flows and heat transport in the gas is based on the numerical solution of the system of equations for unsteady convective heat transfer, which can be written in the form

$$\frac{\partial(\rho u)}{\partial t} = -\frac{\partial p}{\partial x} + \frac{2}{3\mathrm{Re}}\frac{\partial}{\partial x}\left[\mu\left(\frac{\partial u}{\partial x} - \frac{u}{x} - \frac{\partial w}{\partial z}\right)\right] - \frac{\partial(\rho u^2)}{\partial x} + \frac{2\mu}{\mathrm{Re}\,x}\left(\frac{\partial u}{\partial x} - \frac{u}{x}\right) + \frac{1}{\mathrm{Re}}\frac{\partial}{\partial z}\left[\mu\left(\frac{\partial u}{\partial z} + \frac{\partial w}{\partial x}\right)\right] - \frac{\rho u}{x} - \frac{\partial(\rho u w)}{\partial z}; \quad (1)$$

Moscow. Translated from Zhurnal Prikladnoi Mekhaniki i Tekhnicheskoi Fiziki, No. 5, pp. 100-110, September-October, 1976. Original article submitted September 12, 1975.

$$\frac{\partial(\rho w)}{\partial t} = -\frac{\partial p}{\partial z} - \rho c_F g_z + \frac{2}{3\mathrm{Re}}\frac{\partial}{\partial z}\left[\mu\left(2\frac{\partial w}{\partial z} - \frac{\partial u}{\partial x} - \frac{u}{x}\right)\right] + \frac{1}{\mathrm{Re}}\frac{\partial}{\partial x}\left[\mu\left(\frac{\partial w}{\partial x} + \right.\right.$$

$$\left.\left. + \frac{\partial u}{\partial z}\right)\right] + \frac{\mu}{\mathrm{Re}\, x}\left(\frac{\partial w}{\partial x} + \frac{\partial u}{\partial z}\right) - \frac{\partial(\rho u w)}{\partial x} - \frac{\rho u w}{x} - \frac{\partial(\rho w^2)}{\partial z};$$

$$\frac{\partial \rho}{\partial t} = -\frac{\partial(\rho u)}{\partial x} - \frac{\rho u}{x} - \frac{\partial(\rho w)}{\partial z};$$

$$\frac{\partial(\rho c_p T)}{\partial t} = \frac{1}{\mathrm{Re}\,\mathrm{Pr}}\left[\frac{\partial}{\partial x}\left(\lambda\frac{\partial T}{\partial x}\right) + \frac{\lambda}{x}\frac{\partial T}{\partial x} + \frac{\partial}{\partial z}\left(\lambda\frac{\partial T}{\partial z}\right)\right] - \frac{\partial(\rho u c_p T)}{\partial x} -$$

$$-\frac{\rho u c_p T}{x} - \frac{\partial(\rho w c_p T)}{\partial z} + \mathrm{Ec}\, R^*\left[\rho\left(u\frac{\partial T}{\partial x} + w\frac{\partial T}{\partial z}\right) - \rho T\left(\frac{\partial u}{\partial x} + \frac{u}{x} + \frac{\partial w}{\partial z}\right)\right] + \mathrm{Ec}\frac{\mu}{\mathrm{Re}}\Phi,$$

where

$$\Phi = \left\{2\left[\left(\frac{\partial u}{\partial x}\right)^2 + \left(\frac{u}{x}\right)^2 + \left(\frac{\partial w}{\partial z}\right)^2\right] - \frac{2}{3}\left(\frac{\partial u}{\partial x} + \frac{u}{x} + \frac{\partial w}{\partial z}\right)^2 + \left(\frac{\partial u}{\partial z} + \frac{\partial w}{\partial x}\right)^2\right\};$$

t is the time; u and w are, respectively, the x and z components of the velocity v'; p is the pressure; ρ is the density; T is the temperature; and Φ is the dissipation function. The temperature is measured in units of the temperature difference between the hot and cold surfaces $\Delta T' = T'_2 - T'_1$ (from now on dimensional quantities are denoted by primes), and the velocity unit is the velocity of sound $V' = \sqrt{\varkappa R^* T_m}$ at the average temperature over the gap $T'_m = \frac{T'_1 + T'_2}{2}$ under conditions of hydrostatic equilibrium in the absence of body forces. The units of density, specific heat, dynamic viscosity, and thermal conductivity are their values at the temperature T'_m. The unit of length is taken as the thickness of the layer $\delta' = r'_2 - r'_1$, the time scale as $\delta'/(V')^2$, pressure as $\rho_m (V')^2$, and gravity as g'. The dimensionless groups appearing in the equations have the form

$$\mathrm{Re} = V'\delta'/\nu', \; c_F = g'\delta'/(V')^2, \; \mathrm{Ec} = (V')^2/c'_{pm}\Delta T'.$$

Steady-state distributions of velocity, density, and temperature are reached at $t \to \infty$. We assume that at zero time the gas is stationary over the whole region $(u = w = 0)$.

For given constant temperatures on the boundaries of the region $r = r_1$, $T = T_1$; $r = r_2$, $T = T_2$ the temperature within the layer varies only along the radius and is given by the heat-conduction equation

$$\frac{\partial}{\partial x}\left(\lambda\frac{\partial T}{\partial x}\right) + \frac{\partial}{\partial z}\left(\lambda\frac{\partial T}{\partial z}\right) + \frac{\lambda}{x}\frac{\partial T}{\partial x} = 0.$$

The density at $t = 0$ is determined by the equation of state in accord with the given temperature distribution. The boundary conditions on the spherical surfaces are taken as

$$r = r_1, \; r = r_2, \; u = w = 0,$$

where r is the running value of the radius; the density is calculated from the equation of continuity, taking account of the boundary conditions for the velocity components.

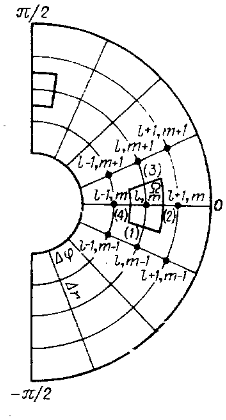

Fig. 1

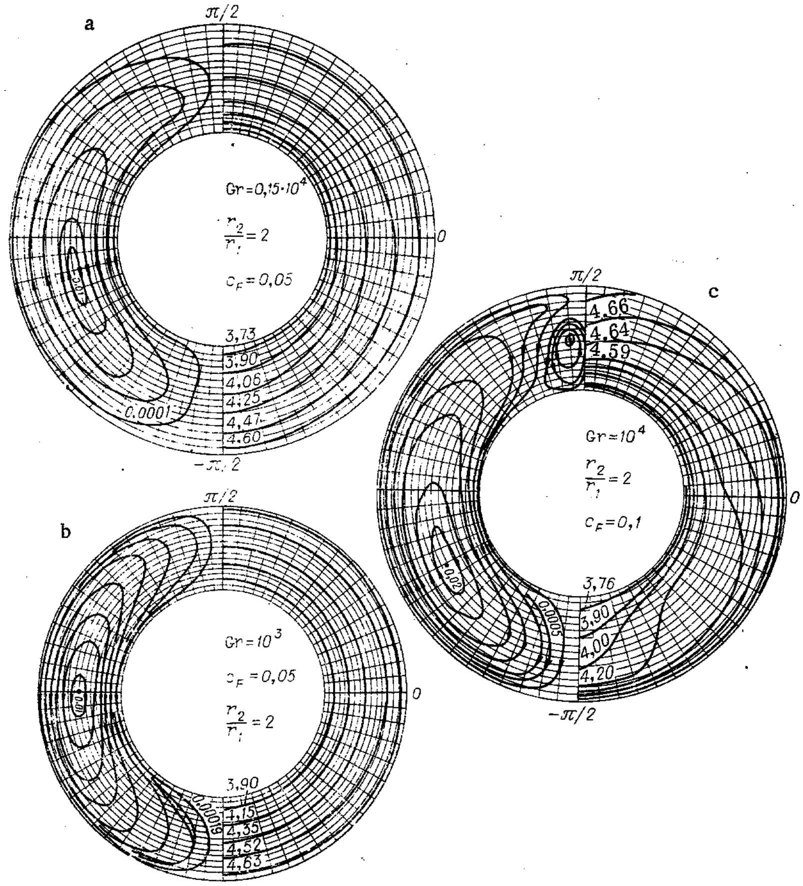

Fig. 2

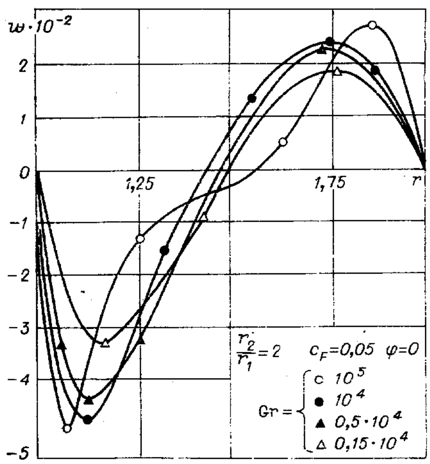

Fig. 3

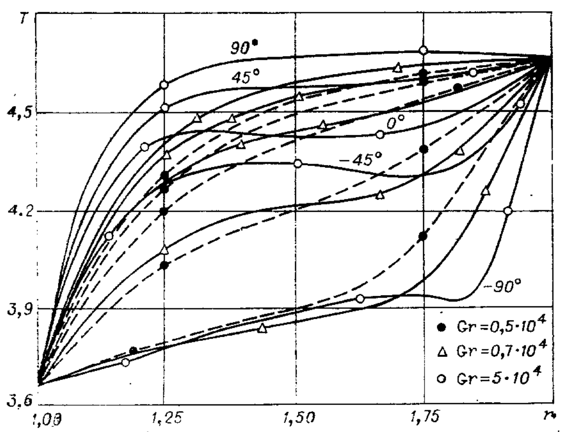

Fig. 4

For constant temperatures of the spherical surfaces, the steady-state flow and heat transfer depend on the following dimensionless quantities: the Grashof number $\mathrm{Gr} = g'\beta_m' \Delta T' \delta^{1/3}/(\nu_m')^2$, the Prandtl number $\mathrm{Pr} = \mu_m' c_{pm}'/\lambda_m'$, the hydrostatic compressibility criterion c_F, the ratio of the radii of the spheres r_2/r_1, and the ratio of the specific heats $\varkappa = c_p'/c_v'$. We have investigated the effect of the Grashof number and the ratio of the radii r_2/r_1 on flow and heat transfer. The values of the rest of the governing criteria were fixed: $\mathrm{Pr} = 0.71$, $\varkappa = 1.4$, $c_F = 0.05$. In the calculations the variation of the Gr number for a fixed value of c_F was achieved by varying the Re number in accord with the expression $\mathrm{Re} = \sqrt{(\mathrm{Gr}/c_F)\,T_m}$.

The limiting time-independent solution of the system of nonlinear differential equations (1) was found by an explicit difference scheme with correction at each time step [7]. The existence and uniqueness of the solution for given boundary and initial conditions follow from the physical meaning of the problem.

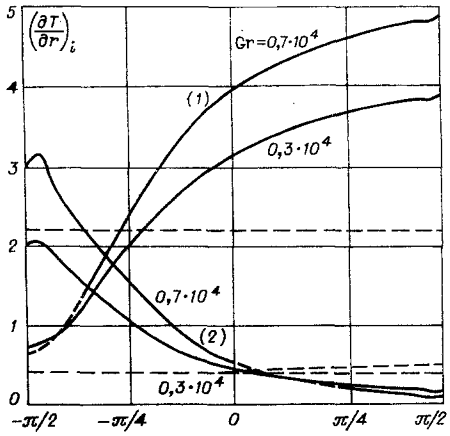

Fig. 5

TABLE 1

Mesh $l\times m$	ε_{h1}	ε_{h2}	Discrepancy, %	ε_h
17×17	1,3150	1,3418	2	1,3284
31×31	1,4747	1,4921	1,2	1,4834
17×33	1,4855	1,4929	0,5	1,4892

The system of difference equations was obtained by the method of balances, which essentially consists in integrating each equation of the original system (1) over a cell of the region and then replacing the integrals by finite sums. The finite-difference equations are written in operator form, which greatly simplifies the programming for the computer.

We analyze the method of obtaining the difference equations by the example of a quasilinear first-order differential equation depending on two spatial variables and written in the form of a divergence

$$a_0 \frac{\partial v}{\partial t} + \frac{\partial}{\partial x_j}\left(a_{jk} \frac{\partial v}{\partial x_k}\right) = 0, \qquad k = 1,\ 2, \tag{2}$$

where the x_j are Cartesian coordinates, and the $a_{jk} = a_{jk}(v, x, t)$ are smooth functions in the closed domain R within which the solution of Eq. (2) is sought.

We introduce in domain R an orthogonal curvilinear coordinate system z_i, chosen because of the geometry of the region and the form of the boundary conditions for Eq. (2).

The coordinate lines z_i = const form a curvilinear orthogonal mesh in domain R with L nodes along z_1 and N along z_2. We choose four arbitrary cells of the mesh having a common node, such as the one with coordinates $z_{1l} = l h_1$, $z_{2m} = mh_2$; h_1 and h_2 are, respectively, the mesh sizes in the z_1 and z_2 directions. The form of the mesh and the numbering of the nodes are shown in Fig. 1.

Let Ω be an auxiliary cell with its center at $(z_{1l},\ z_{2m})$ and sides passing through the nodes with coordinates

$$(z_{1l+1/2},\ z_{2m}),\ (z_{1l},\ z_{2m+1/2}),\ (z_{1l},\ z_{2m-1/2}),\ (z_{1l-1/2},\ z_{2m}).$$

The half-integral subscripts denote, for example,

$$z_{1l+1/2} = lh_1 + h_1/2;\ z_{2m-1/2} = mh_2 - h_2/2.$$

We integrate Eq. (2) over cell Ω and approximate the integrals on the right-hand side of the equation by using Green's theorem. In operator form we can write

$$\iint\limits_{\Omega} \frac{\partial W}{\partial x_j} d\Omega = \oint W n_j ds,$$

where n_j is the x_j component of the outward normal to contour Γ of cell Ω.

For convenience in writing, we number the sides of Ω as shown in Fig. 1. We denote by W_k the value of the integrand on the k-th side (k = 1, 2, 3, 4), and by $W_{l,m}$ its value at the node $(lh_1,\ mh_2)$.

Along side k we treat W_k as constant and equal to its value at the node with the half-integral subscripts, where W_k is calculated by the symmetric formula, e.g.,

$$W_1 = W_{l+1/2,\ m} = (W_{l,\ m} + W_{l+1,m})/2. \tag{3}$$

We describe the contour integral along the sides of Ω by using (3). At the same time we transform from coordinates x_j to z_i. Then

$$\oint W n_j ds = W_1 \int_{\Gamma_1} n_{j1} H_1^1 dz_1 + W_3 \int_{\Gamma_3} n_{j3} H_3^1 dz_1 + W_2 \int_{\Gamma_2} n_{j2} H_2^2 dz_2 + W_4 \int_{\Gamma_4} n_{j4} H_4^2 dz_2, \tag{4}$$

where H^1 and H^2 are the Lamé coefficients for the system z_i. In calculating with (4) it is necessary to make sure that $H_k^i dz_i > 0$.

It follows from (2) that W in Eq. (4) depends linearly on derivatives which are calculated by the formula [8]

$$\partial/\partial x_j = (l_{ij}/H^i)\partial/\partial z_i, \tag{5}$$

where l_{ij} is the x_j component of the unit vector tangent to the coordinate line z_i. Using (5) we have

$$\int_\Gamma \left(a_{jk} \frac{\partial v}{\partial x_k}\right) n_j ds = \int_\Gamma a_{jk} n_j \left(\frac{l_{ij}}{H^i} \frac{\partial v}{\partial z_i}\right) ds.$$

The integral on the right-hand side is evaluated by parts along each side i of cell Ω. The derivatives in (5) were determined by the symmetric formulas ensuring the approximation of $\partial/\partial x_j$ to second-order accuracy. For example,

$$\partial v/\partial z_1 = (v_{l,\ m+1} - v_{l,\ m-1} + v_{l+1,\ m-1} - v_{l-1,\ m-1})/4h_1;$$
$$\partial v/\partial z_2 = (v_{l+1,\ m} - v_{l,\ m})/h_2.$$

In the problem under consideration the space cell $\overline{\Omega}$ is chosen as follows. We divide the region between the spheres into sectors by planes R_θ passing through the axis of symmetry with an angle $\Delta\theta$ between them. Because of the symmetry of the problem it is sufficient to find the solution in one sector. We seek the solution in the sector bounded by the planes R_0 and R_θ which correspond to the angles $\theta = 0$ and $\theta = \Delta\theta$. We introduce polar coordinates r and φ in the R_0 plane. Then the sides of the space cell $\overline{\Omega}$ are formed by the sides of Ω (Fig. 1) by rotating the R_0 plane through an angle $\Delta\theta$ about the z axis. The lateral sides of $\overline{\Omega}$ lie in the planes R_0 and R_θ of the sector in which the solution is being determined. The cells $\overline{\Omega}$ directly adjacent to the axis of symmetry are formed by rotating the half cell Ω by $\Delta\theta$. To save space the integral notation of the equations is not presented. Because of the symmetry of the problem, the integrand does not depend on θ and

$$\int\iint_{\overline{\Omega}} \frac{\partial W}{\partial X} x dx dz d\theta = \Delta\theta \iint_{\Omega} \frac{\partial W}{\partial X} x dx dz,$$

where X is any of the coordinates t, r, z. The methods of evaluating the contour integrals for cells on the z axis ($\varphi = \pm\pi/2$) and for those at a distance from it ($-\pi/2 < \varphi < +\pi/2$) are different. For $-\pi/2 < \varphi < +\pi/2$ we have

$$\iint_\Omega \frac{\partial (Wx)}{\partial x} dx dz = \int_\Gamma (Wx) n_x ds = \left[(W_1 x_1 - W_3 x_3)\cos\frac{\Delta\varphi}{2}\cdot\sin\varphi - \right.$$
$$\left. - (W_1 x_1 + W_3 x_3)\cos\varphi \sin\frac{\Delta\varphi}{2}\right]\Delta r + \left[(W_2 x_2 - W_4 x_4) r + \right.$$
$$\left. + (W_2 x_2 + W_4 x_4)\frac{\Delta r}{2}\right]\cos\varphi\cdot\sin\varphi + \left(\frac{\Delta\varphi}{2} - \frac{\sin\Delta\varphi}{2}\right)\left[W_2\left(r + \frac{\Delta r}{2}\right)^2 - W_4\left(r - \frac{\Delta r}{2}\right)^2\right];$$

$$\iint_\Omega \frac{\partial (Wx)}{\partial z} dx dz = \int_\Gamma (Wx) n_z ds = \left[(W_2 x_2 - W_4 x_4) r + (W_2 x_2 + W_4 x_4)\frac{\Delta r}{2}\right]\times$$
$$\times \sin^2\Delta\varphi - \left[(W_1 x_1 - W_3 x_3)\cos\varphi\cdot\cos\frac{\Delta\varphi}{2} + (W_1 x_1 + W_3 x_3)\sin\varphi \sin\frac{\Delta\varphi}{2}\right]\Delta r.$$

For $\varphi = +\pi/2$

$$\iint_\Omega \frac{\partial (Wx)}{\partial x} dx dz = (W_1 x_1)\Delta r \cos\frac{\Delta\varphi}{2} + \left[W_2\left(r + \frac{\Delta r}{2}\right)^2 - W_4\left(r - \frac{\Delta r}{2}\right)^2\right]\left(\frac{\Delta\varphi - \sin\Delta\varphi}{2}\right);$$

$$\iint\limits_{\Omega} \frac{\partial (Wx)}{\partial z}\, dxdz = -(W_1x_1)\Delta r \sin\frac{\Delta\varphi}{2} + \left[W_2\left(r+\frac{\Delta r}{2}\right)^2 - W_4\left(r-\frac{\Delta r}{2}\right)^2\right]\frac{\sin^2\Delta\varphi}{2}.$$

The difference expressions for $\varphi = -\pi/2$ are written similarly.

The numerical solution enables one to obtain the hydrodynamic structure of the flow and the pattern of the temperature distribution $T(r, \varphi)$ for various flow regimes characterized by the Grashof number Gr and the ratio of the radii r_2/r_1. Knowing the temperature distribution, the local Nusselt numbers $(\partial T/\partial r)_i$ at the boundaries of the region can be calculated, and then the convection coefficient ε_{ki} is given by the expression

$$\varepsilon_{ki} = \frac{\lambda_s}{\lambda_m} = \lambda_i \frac{r_i^2}{r_1 r_2}\left(\frac{\partial \overline{T}}{\partial r}\right)_i, \tag{6}$$

which shows the excess of convective heat transfer over pure conduction.

In Eq. (6), $(\partial \overline{T}/\partial r)_i$ is the average value of the Nusselt number over the boundary of the region and is equal to

$$\left(\frac{\partial \overline{T}}{\partial r}\right)_i = \frac{1}{2}\int\limits_{-\pi/2}^{+\pi/2}\left(\frac{\partial T}{\partial r}\right)_i \cos\varphi d\varphi,\ i = 1, 2.$$

The derivative in the last expression was approximated by the three-point formulas giving second-order accuracy of the form

$$\partial T/\partial r \simeq (3T_{l-1,\, m} - 4T_{l,\, m} + T_{l+1,\, m})/2\Delta r.$$

Using the difference method described, a BÉSM–ALGOL program was written for a BÉSM-6 computer and translator connected to a "Dubna" monitor system. The machine time required with this arrangement was shorter than with an ordinary ALGOL translator by a factor of 2.2.

The main results presented below were obtained with an $N_r \times N_\varphi = 17 \times 33$ mesh. This mesh was optimum from the point of view of admissible calculational error and the necessary expenditure of machine time. To justify the choice of the numbers of nodes of the difference mesh along the different coordinate axes we performed calculations with 17×17, 17×33, and 31×31 meshes. The effect of the mesh size on the convection coefficient can be judged from the data of Table 1 obtained for $Gr = 0.5 \cdot 10^4$, $c_F = 0.05$, and $r_2/r_1 = 2$. The data in Table 1 correspond to the steady state. In a calculation without error $\varepsilon_{k1} = \varepsilon_{k2}$. The discrepancy is defined as $\Delta\varepsilon = (|\varepsilon_{k2} - \varepsilon_{k1}|/\varepsilon_{k2})\,100\%$.

A comparison of the convection coefficients for $l \times m = 17 \times 17$ and $l \times m = 31 \times 31$ shows that the discrepancy is not always significantly decreased simply by increasing the number of nodes. This effect can be explained by the nonuniformity of the mesh resulting from the curvilinear nature of the region.

In choosing a uniform mesh $(l - 1 = m - 1)$ it is assumed that a cell Ω will be nearly square, but actually it depends on the position of the cell along the radius. The degree of distortion of the cell is characterized by the deviation of the ratio of the sides of the cell from unity

$$K = \Delta r/r\Delta\varphi = \delta(m-1)/(l-1)r\pi,$$

where $l - 1$ is the number of Δr steps along the radius, and $m - 1$ is the number of $\Delta\varphi$ steps in angle from $\varphi = -\pi/2$ to $\varphi = +\pi/2$.

When $\delta = 1$ this relation reduces to

$$K = (m-1)/(l-1)r\pi. \tag{7}$$

Hence when $l - 1 = m - 1$ we obtain $K = 1/r\pi$; i.e., the distortion does not depend on the number of nodes along r and φ and is minimum for $r = 1/\pi = 0.32$.

The data in Table 1 were obtained for a ratio of the radii $r_2/r_1 = 2$, which for $\delta = 1$ leads to the relation $1 \le r \le 2$, and, consequently, $1/2\pi \le K \le 1/\pi$. Clearly, it is necessary to take $l - 1 \ne m - 1$ to decrease the distortion of the cell. The optimum mesh, determined by the ratio $(m-1)/(l-1)r\pi$ for $1 \le r \le 2$, satisfies the inequality $\pi \le (m-1)/(l-1) \le 2\pi$, which shows that on the average the number of nodes along φ must be approximately 4.5 times as large as the number along r.

Because of the limitations of the computer memory the total number of nodes is ordinarily kept constant, $l \times m = \text{const}$. For a ratio of steps Δr and $\Delta\varphi$ determined by Eq. (7) the error in the approximation of the derivative with respect to r is appreciably increased, and this has an adverse effect on the results of the calculation. The optimum mesh is chosen by a careful numerical experiment. In our case $N_r \times N_\varphi = 17 \times 33$, for which the ratio $(m-1)/(l-1) = 2$.

With $Gr \leq 10^4$ this mesh leads to a discrepancy of about 0.5%. As Gr is increased the discrepancy increases rapidly, and for $Gr = 0.5 \cdot 10^5$ and 10^5 it reaches 7 and 9%, respectively. This increase in discrepancy, and, consequently, in the error of the calculation, is accounted for in the present case by the complication of the flow structure. For these Gr numbers a secondary eddy is formed in the neighborhood of $\varphi = +\pi/2$. A weaker eddy appears at $\varphi = -\pi/2$, close to the outer and inner spheres.

The numerical solution required 2-3 calculational nodes along r in the region of the secondary eddy, i.e., the mesh was very coarse, particularly if the eddy did not extend over the whole width of the gap. This fault was eliminated by changing to a finer 31×33 mesh, although such a fine mesh was not required for most of the computational region. A more reasonable approach is clearly to compress the mesh in r and φ in the neighborhood of the verticals $\varphi = \pm\pi/2$. This decreases the calculational error without increasing the total computation time too much.

The time step is determined by the stability conditions

$$\Delta t \leqslant \min\,(h^2/4\nu,\ h/|a|)$$

(or $\Delta t \leq h/|a|$, since generally $h/|a| \ll h^2/4\nu$), obtained by Fourier methods for the model equation $\partial u/\partial t = a\,\partial u/\partial x + \nu\,\partial^2 u/\partial x^2$, where a is a quantity related to the maximum of the velocities u, w; ν is a constant determined by the maximum value of the kinematic viscosity.

To obtain the velocity and temperature distribution patterns and the dependence of the convection coefficient on the governing criteria, calculations were performed in which the Grashof number and the ratio of the radii were varied between the following limits: $10^3 \leq Gr \leq 10^5$, $1.2 \leq r_2/r_1 \leq 3$.

The nature of the motion generated in the layer and the characteristics of the temperature distribution can be judged from Fig. 2 which shows the flow lines ψ and the isotherms for several values of the Grashof number. Convection hardly affects the heat transfer for $Gr = 10^3$, although Fig. 2a clearly shows the presence of ascending and descending flows. The total amount of heat transferred in this case is by conduction, as is confirmed by the value of 0.98 for the convection coefficient.

For $Gr = 10^3$ the isotherms are practically circles, but with increasing values of the Grashof number they are distorted (Fig. 2b), and for $Gr = 10^4$ they undergo a pronounced change (Fig. 2c). This is related to the character of the motion in the gap. The gas rises along the heated outer sphere and descends along the cooled inner sphere. In this case unicellular flow (crescent eddy) occurs for all the values of r_2/r_1 and Grashof numbers $Gr < 10^5$ considered. The secondary eddy which appears at the inner sphere near the vertical $\varphi = \pm\pi/2$ for $Gr = 10^4$ is small and localized, and therefore is assumed to be unicellular also. As the Grashof number is increased for a constant ratio r_2/r_1 the intensity of the circulation in the gap increases and eddy center is displaced downward at an angle (Fig. 2a-c).

In this type of flow the gas in the eddy part of the region heats up more strongly, and the isotherms here are rather far away from the outer wall (Fig. 2c) and bunched close to the inner wall. The opposite effect is observed in the lower part of the region; the cooled gas lowers the temperature of the inner sphere. At the outer sphere the heated gas is carried upward by the flow, and the isotherms are close to the wall.

For $Gr = 10^4$, corresponding to a rather well-developed convection regime, thermal and velocity boundary layers are formed close to the spheres. The formation of a boundary layer and the flow core with increasing Grashof number can be traced in Fig. 3. The curves are plotted for $r_2/r_1 = 2$. Figure 3 shows the profile of the vertical component of velocity w at $\varphi = 0$ for various values of the radius r. In regions adjoining the spheres the gas has a high flow velocity as compared with the velocity in the central and main parts of the eddy. This effect increases as Gr approaches the maximum values considered. The maximum velocity of the ascending flow w_2 occurs at a distance from the boundary which is large in comparison with that of the maximum velocity w_1 of the descending flow, since the outer heated wall has a larger area than the cold inner wall, and the dynamic layer of gas is thicker here.

Figure 4 shows the temperature profile as functions of the radius for various values of the angle φ. Temperature stratification with a central zone where the temperature gradient is small and relatively uniform is characteristic for convection. This portion corresponds to the central low-velocity part of the eddy where heat is transferred mainly by conduction. Most of the heat transfer is concentrated close to the boundaries of the region where the gradient along the radius is large. As φ increases from $-\pi/2$ to $\pi/2$ the value of the steep increase of the gradient at the inner sphere increases, and the value at the outer sphere decreases. This kind of profile results from the high rate of heat transfer in the tangential direction in the high-velocity boundary layer. The shape of the profile for a corresponding value of the angle remains essentially unchanged for a change in the ratio r_2/r_1, and only the temperature changes for a given radius and extension of the characteristic parts of the profile along r. All these properties of the profiles are confirmed qualitatively by experiment [3].

Processing the results of the numerical solution by similarity theory methods gives the following expression for the convection coefficient ε_k as a function of the Rayleigh number Ra:

$$\varepsilon_k = 0.143 \cdot \mathrm{Ra}^{0.273} \tag{8}$$

in the range $7 \cdot 10^2 \le \mathrm{Ra} \le 7 \cdot 10^4$ and $1.2 \le r_2/r_1 \le 3$. The corresponding experimental formula for a spherical layer obtained in [3] is

$$\varepsilon_k = 0.12 \cdot \mathrm{Ra}^{0.276}.$$

It is valid in the range $1.4 \cdot 10^4 \le \mathrm{Ra} \le 2.5 \cdot 10^6$, $\mathrm{Pr} = 0.71$, and $1.09 \le r_2/r_1 \le 2.81$. The similarity criteria are the same in both cases.

In addition to the integral heat-transfer characteristics, the local heat fluxes at the outer and inner spheres were calculated and plotted in Fig. 5 for two values of the Grashof number. The dashed lines show the heat flux in a stationary gas. The value of $(\partial T/\partial r)_i$ $(i = 1, 2)$ decreases in the direction of flow and becomes smaller than in heat conduction, since the gas gradually acquires a temperature close to that of the surface along which it moves. Comparisons for various values of the Gr number show that the maximum values of the heat fluxes increase with increasing Gr.

The following conclusions can be drawn from the results obtained: in the range of Gr numbers and ratios of radii considered there is stable single-eddy motion; the convection coefficient varies slowly with the ratio r_2/r_1; ε_k can be calculated from Eq. (8) which depends only on the Rayleigh number.

LITERATURE CITED

1. D. I. Boyarintsev, "Heat transfer through liquid and gaseous layers," Zh. Tekh. Fiz., 20, No. 9 (1950).
2. E. H. Bishop, R. S. Kolflat, L. R. Mack, and J. A. Scanlan, "Convective heat transfer between concentric spheres," in: Proceedings of 1964 Heat Transfer and Fluid Mechanics Institute, Stanford University Press (1964).
3. J. A. Scanlan, E. H. Bishop, and R. E. Powe, "Natural convection heat transfer between concentric spheres," Intern. J. Heat Mass Transfer, 13, 1857 (1970).
4. S. H. Yin, R. E. Powe, J. A. Scanlan, and E. H. Bishop, "Natural convection flow patterns in spherical annuli," Intern. J. Heat Mass Transfer, 16, 1785 (1973).
5. L. R. Mack and H. C. Hardee, "Natural convection between concentric spheres at low Rayleigh numbers," Intern. J. Heat Mass Transfer, 11, 387 (1968).
6. V. V. Barelko and É. A. Shtessel', "Natural convection heat transfer in cylindrical and spherical layers," Inzh.-Fiz. Zh., 24, No. 1 (1973).
7. G. B. Petrazhitskii, E. V. Bekneva, and N. M. Stankevich, "Calculations of flow and heat transfer in the free motion of a liquid in a horizontal annular channel," Trudy L'vovsk. Politekh. Inst., No. 46 (1970).
8. N. E. Kochin, Vector Calculus and the Elements of Tensor Calculus [in Russian], Nauka, Moscow (1965).